JOURNAL OF GEOPHYSICAL RESEARCH, VOL. 102, NO. A12, PAGES 27,217–27,226, DECEMBER 1, 1997

Oblique turbulence driven by field-aligned electron fluxes in the auroral ionosphere

L. Muschietti, I. Roth, and G. Delory

Space Sciences Laboratory, University of California, Berkeley

Abstract. This paper investigates how the various waves of the whistler resonance cone compete for the free energy available in field-aligned fluxes of precipitating electrons in the auroral ionosphere. A two-dimensional numerical simulation code, based on the coupled pair of quasi-linear equations, is used for the investigation. The description provided by these equations allows us to follow the nonlinear development of the instability and analyze the interplay between the modes as mediated by the changing distribution function. We present results for a parameter regime corresponding to altitudes probed by sounding rockets, around 10^3 km and $\Omega_e \gtrsim \omega_p$. The presence of a halo of energetic electrons significantly affects the evolution of the turbulence. The spectrum is shown to shift with time toward increasingly oblique propagation angles including a substantial share of quasi-perpendicular, short-wavelength modes close to the lower hybrid frequency.

1. Introduction

VLF emissions are routinely observed in the auroral ionosphere by rockets and satellites [e.g., *Beghin et al.*, 1989]. The emissions, which are often accompanied by fluxes of precipitating electrons, can be electromagnetic or quasi-electrostatic. In the latter case the waves have been identified as belonging to resonance cones. At altitudes above 1000 km, where the plasma frequency drops below the electron cyclotron frequency, $\omega_p \lesssim \Omega_e$, they belong to the whistler resonance cone [*Beghin et al.*, 1989; *Ergun et al.*, 1993] with frequencies extending from the the lower hybrid resonance (several kilohertz) up to the plasma frequency (about one megahertz). The electron fluxes accompanying the waves are transient, field-aligned, and embedded in a quasi-isotropic nonthermal halo. Presumably they form a bump which destabilizes the waves. Figure 1 shows an example of distribution function $f(v_{||}, v_\perp)$ captured by a sounding rocket during a measurement of short-wavelength VLF emissions in the lower hybrid frequency range. Even though the fast time resolution of the snapshot (128 ms) limits somewhat the particle count, hence the statistics at large velocities, the main features are clearly seen: a field-aligned beam in the downgoing parallel velocities $v_{||} > 0$ and low perpendicular velocities $v_\perp \sim 0$, and a quasi-isotropic halo.

Assuming that the low-frequency waves are due to an electron beam, though, raises a paradoxical point. It is indeed well known that Langmuir waves are the fastest waves to grow off a bump in the distribution function. They may be expected to grow first and via quasi-linear feedback to quickly remove all the free energy available, so that it seems paradoxical that any lower-frequency waves could be seen at all. This is in fact a fairly general point which arises whenever one invokes an electron beam to excite low-frequency waves, for example, electromagnetic ion cyclotron waves in the aurora [*Temerin and Lysak*, 1987] and the solar corona [*Roth and Temerin*, 1997]. Several ideas have been previously suggested to resolve the paradox.

The commonly accepted explanation, at least in the auroral context, relies on the concept of convective growth and goes as follows. Langmuir waves in a magnetized plasma acquire a large perpendicular group velocity as soon as their propagation angle veers a few degrees off the direction of the magnetic field **B**. Thus the waves, which are excited in a perpendicularly finite channel, move rapidly across the field lines and may leave the growth region. By contrast, the lower hybrid waves have their group velocity pointing mostly parallel to **B** and so follow the precipitating beam for a longer time, thereby dominating the emissions in spite of a smaller growth rate [*Maggs*, 1978; *Maggs and Lotko*, 1981; *Retterer et al.*, 1989].

Another idea, considered by *Serizawa and Dum* [1992] is that the finite perpendicular extent of the beam itself may modify the dispersion relation to favor low-frequency, oblique modes rather than Langmuir. Unless the width L_b of the beam is small in terms of parallel wavelength, $k_{||} L_b \lesssim 100$, these authors concluded, the dispersion relation is close to the infinite beam-plasma system, and the growth peaks for parallel propagating modes. For auroral parameters the condition amounts to L_b less than a few hundred meters.

Paper number 97JA02532.
0148-0227/97/97JA-02532$09.00

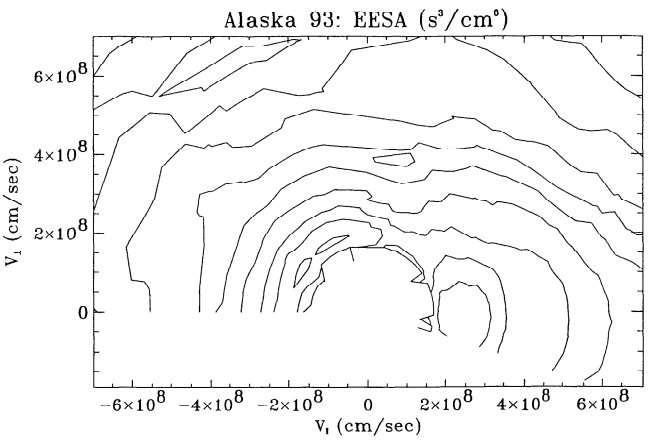

Figure 1. Example of distribution function measured by a sounding rocket (time resolution 128 ms). The contours are logarithmically spaced, two per decade. The core around $v_{||} = v_\perp = 0$ has been truncated. Note the downgoing field-aligned beam about $v_{||} \approx 3 \times 10^8$ cm/s and the hot halo of electrons with large $v_\perp$.

An alternate suggestion explains the low-frequency, oblique waves as being due to the so-called fan instability [*Omelchenko et al.*, 1994]. This instability does not require a bump but necessitates the presence of a long flat tail in the electron distribution function; it is driven through the anomalous Doppler resonance, $(\omega + \Omega_e)/k_{||}$, instead of the main $\omega/k_{||}$ Cerenkov resonance. While the original model was developed in the context of tokomak physics [*Parail and Pogutse*, 1976], where the presence of runaway electrons can add the required flat tail to the distribution function, the application to auroral physics at 1000 km altitudes has not been supported by detailed distribution function measurements. Typical velocities of the electrons resonating with the $n = -1$ anomalous Doppler resonance and with the $n = 0$ Cerenkov resonance are in a ratio $(\omega+\Omega_e)/\omega \sim 0.5\sqrt{M/m} \sim 80$ for lower hybrid waves in an oxygen plasma. Because the observed distributions consist mainly of rapidly falling power laws ($\sim v^{-5}$) [*McFadden et al.*, 1987], the particle flux at the $n = 0$ resonance is many orders of magnitude larger than it is at the $n = -1$ resonance. The stabilizing effect of the Cerenkov electrons is, under these conditions, hard to overcome.

Recently it was emphasized [*Ergun et al.*, 1993] that the beam is in fact a feature embedded in a nonthermal halo (an example is visible in Figure 1); the explanation for the low-frequency waves then goes as follows. If the wavelength of the oblique waves is short enough for some of the halo electrons to have a larger gyroradius, then these electrons "see" all the possible wave phases during one brief gyration time. As a result their interaction with the waves is weak, even if they satisfy the Cerenkov condition $v_{||} = \omega/k_{||}$. In contrast, the Langmuir waves have a very large wavelength in the direction perpendicular to **B**. Hence, even energetic electrons with a large gyroradius remain in the same wavefront and interact strongly with the waves. Due to this difference, oblique waves can be unstable for a distribution function where Langmuir waves are in fact stable.

This last idea is quite interesting from a kinetic viewpoint and may have wider applicability than the auroral region. The purpose of this paper is to explore it further, using the potential of numerical computations. By means of simulations we investigate how the various modes of the resonance cone compete dynamically for the free energy available in a distribution function that is made of a tenuous field-aligned beam embedded in a large halo. Beyond a mere evaluation of linear growth rates we follow the nonlinear development of the instability and analyze the interplay between the modes as mediated by the changing distribution function. It is shown that the spectrum ends up being dominated by the slower growing, oblique modes.

2. Quasi-linear Model

Since the wave spectrum depends upon both $k_{||}$ and $k_\perp$, and since at the Cerenkov resonance $v_0 = \omega/k_{||}$ oblique and parallel modes interact differently with the distribution function, the problem is intrinsically two-dimensional. True, the diffusion associated with the $n = 0$ term, the most important as we shall see, is effectively one-dimensional. Still, the two-dimensionality of the spectrum and distribution function precludes the reduction to a one-dimensional problem with a one-to-one correspondence between spectrum and distribution function. Electrons at a given $(v_{||}, v_\perp)$ depend on an integral over the spectrum that includes all the modes satisfying $\omega/k_{||} = v_{||}$, i.e. a sinuous line in $(k_{||}, k_\perp)$ space. One can see an example of the line in Figure 2.

Rather than cope with the multiple compromises of a two-dimensional particle-in-cell code (see *Dum and Nishikawa* [1994] for an account of the limitations on present-day supercomputers), we opted for the description of wave-particle interactions offered by the coupled pair of magnetized quasi-linear equations. This approach allows us to simultaneously treat the interactions (at a much lower and more realistic wave level), handle the wide range of particle densities in phase space that is required by the problem, and follow the evolution over timescales of the order of $10^6\ \omega_p^{-1}$.

2.1. Coupled Pair of Equations

Let $f(v_{||}, v_\perp, t)$ be the electron distribution function and $W_k(k_{||}, k_\perp, t)$ be the wave intensity spectrum ($W_k = |E_k|^2$); their joint evolution is modeled by numerically integrating the set

$$\frac{\partial f}{\partial t} = \pi \left(\frac{e}{m}\right)^2 \sum_n \int \frac{d^3k}{(2\pi)^3}\, \hat{L}_n \frac{W_k}{k^2}\, J_n^2\left(\frac{k_\perp v_\perp}{\Omega_e}\right) \times \delta(\omega - k_{||}v_{||} - n\Omega_e)\hat{L}_n f, \quad (1)$$

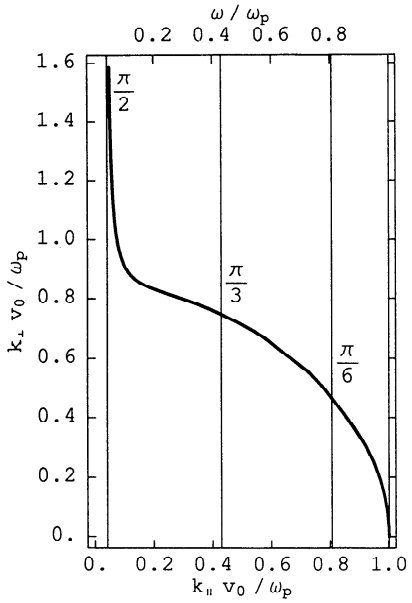

Figure 2. Loci of the modes $(k_{||}, k_\perp)$ that satisfy the resonance $\omega = k_{||} v_0$ for a given v_0. The thin vertical lines indicate four propagation angles (0°, 30°, 60°, and 90°). From the parallel Langmuir waves to the nearly perpendicular lower hybrid waves a whole range of wavenumbers can simultaneously be excited. The scale on the upper edge yields the frequency.

$$\frac{\partial W_k}{\partial t} = W_k \frac{2\pi}{k^2 \partial\epsilon/\partial\omega} \sum_n \int d^3v J_n^2 \left(\frac{k_\perp v_\perp}{\Omega_e}\right) \times \delta(\omega - k_{||} v_{||} - n\Omega_e) \hat{L}_n f, \quad (2)$$

where $\hat{L}_n$ is used to denote the differential operator $\hat{L}_n \equiv k_{||}\partial/\partial v_{||} + (n\Omega/v_\perp)\partial/\partial v_\perp$. The notation in (1) and (2) is standard, and we note only that cylindrical symmetry is assumed. Because of the ordering $\Omega_e^{-1} \ll \tau_{ac} \ll \tau_{diff}$, where τ_{ac} is the autocorrelation time and τ_{diff} is the diffusion time (i.e., timescale over which f evolves), gyrotropy can be safely assumed. The numerical discretization of (1) and (2) relies on the finite element method, which has proven convenient for a consistent treatment of the resonant delta functions [*Appert et al.*, 1976; *Succi*, 1987]. Inhomogeneous grids are used to allow us to cover broad ranges in v and k spaces with sufficient resolution in the interesting regions.

2.2. Dispersion Relation

At altitudes of the order of 1000 km the electron density is overwhelmingly dominated by the cold population, therefore it is sufficient to use the cold dielectric approximation

$$\epsilon = 1 - \frac{\omega_p^2}{\omega^2}\left(\frac{k_{||}^2}{k^2} + \frac{m}{M}\right) - \frac{\omega_p^2}{\omega^2 - \Omega_e^2}\frac{k_\perp^2}{k^2}, \quad (3)$$

where m and M are the masses of the electron and ion, respectively. Equation (3) provides the real frequency ω as well as the factor $\partial\epsilon/\partial\omega$ associated with each pair $(k_{||}, k_\perp)$, quantities that are needed to evaluate (1) and (2). Because $\Omega_e > \omega_p$, we ignore the upper hybrid branch whose modes cannot be destabilized due to a heavy cyclotron damping on the core [*Beghin et al.*, 1989]. The frequency of the electrostatic whistler branch is explicitly given by

$$\omega^2 = \frac{(\Omega_e^2 + \omega_p^2)}{2}\left[1 - \left(1 - \frac{4\Omega_e^2\omega_p^2(\cos^2\theta + m/M)}{(\Omega_e^2 + \omega_p^2)^2}\right)^{1/2}\right], \quad (4)$$

where θ is the angle between the propagation angle and **B**. One usually expands (4) into

$$\omega^2 = \omega_{lh}^2 [1 + \cos^2\theta\,(M/m)], \quad (5a)$$

defining the lower hybrid frequency

$$\omega_{lh}^2 = \frac{\omega_p^2\,(m/M)}{1 + \omega_p^2/\Omega_e^2}. \quad (5b)$$

With a ratio $\Omega_e/\omega_p = 1.5$, which is adopted as our canonical value in this paper, the above expansion (equation (5a)) is accurate for $\theta > 30°$. For smaller angles it underestimates the wave frequencies by as much as 10–20%. Using the exact equation (4), we can find in $(k_{||}, k_\perp)$ space the loci of all the modes that satisfy the Cerenkov condition for a fixed $v_0 = \omega/k_{||}$. Figure 2 displays the resulting resonant line. The normalization used for the wavenumber, $k_{||} v_0/\omega_p$, is such that the horizontal axis also measures the frequency in units of ω_p. The larger values of $k_\perp$ are chosen to accommodate the very oblique eigenmodes close to the lower hybrid frequency. A mass ratio $M/m = 400$ has been assumed for drawing the plot, so the frequencies vary by a factor of 20. This specific choice is dictated by the simulations to be presented in section 3. For larger (and realistic) mass ratios the lower hybrid frequency decreases further, as indicated by (5b); hence the low-frequency, vertical section of the resonant line comes closer to the left edge of the plot. The thin vertical lines show four specific propagation angles ($\theta = 0°$, 30°, 60°, and 90°). The frequency dependence is indicated by the scale at the top of the plot. Let us now analyze the energy transfers associated with various modes chosen along the resonant line.

2.3. Energy Transfers

Quasi-linear theory expresses the energy transfer rate from a set of waves W_k to a population of particle species j as [e.g., *Dum*, 1978]

$$\mathcal{K}_j = 2\int \frac{d^3k}{(2\pi)^3} W_k\, \omega_k\, \mathrm{Im}\, \chi_j(k, \omega_k). \quad (6)$$

For electrons ($j = e$), χ_e is the electron susceptibility of the mode k, whose imaginary part evolves according

to the gradients of f determined from (1),

$$\text{Im } \chi_e(k,\omega_k) = -\pi \left(\frac{\omega_p}{k}\right)^2 \sum_n \int dv_{||}\, dv_\perp v_\perp \times J_n^2\left(\frac{k_\perp v_\perp}{\Omega_e}\right) \delta(\omega_k - k_{||}v_{||} - n\Omega_e)\, \hat{L}_n f. \quad (7)$$

For the sake of definiteness it is convenient at this point to examine a distribution function. An example of our modeling is shown in Figure 3, which displays log f by means of contour lines. The function drops by 2 orders of magnitude every five contours. One distinguishes three components: a Maxwellian core of density n_0 and thermal spread v_e, an isotropic hot halo, and a tenuous beam, namely, $f \equiv f_0 + f_T + f_b$. The halo is described by the generalized Lorentzian,

$$f_T = 1.5\, a^2 n_T (a^2 + v_{||}^2 + v_\perp^2)^{-5/2} \quad (8a)$$

where a is a measure of the spread and the normalization $n_T = \int dv_{||} dv_\perp v_\perp f_T$ is introduced. The beam is described by a drifting, bi-Maxwellian

$$f_b = \frac{n_b}{(2\pi v_{b||}\, v_{b\perp}^2)^{1/2}} \exp[-0.5(v_{||} - U)^2/v_{b||}^2] \times \exp(-0.5\, v_\perp^2/v_{b\perp}^2), \quad (8b)$$

in which U is the drift velocity. Note how in Figure 3 the beam just emerges from the halo and produces a positive slope $\partial f/\partial v_{||} > 0$ near $v_{||} \sim 20\ v_e$ for small values of $v_\perp$. For $v_\perp > 7\ v_e$ the halo takes over, resulting in $\partial f/\partial v_{||} < 0$. For each k mode the integral over $v_\perp$ in (7) averages the slopes and determines the sign of Im χ_e, indicating the direction of the energy flow: from the wave to the electrons or vice versa. Now the various modes along the resonant line of Figure 2 have different $k_\perp$; thus they bias differently the averaging process through the Bessel function $J_0(k_\perp v_\perp/\Omega_e)$. In particular, the low-frequency, oblique waves with a large $k_\perp$ emphasize the features of f at small $v_\perp$. This emphasis leads to an interesting interplay between the modes. As we shall see below, there are periods during the simulation when growing oblique modes reduce the positive slope in the small-$v_\perp$ region, leading to damping previously excited parallel modes.

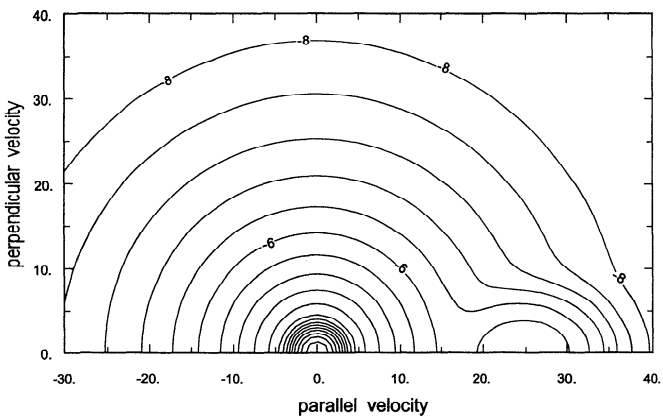

Figure 3. Distribution function used in the simulations. Contours are logarithmically spaced starting from 10^{-8} up, increasing by 2 decades every five contours. Here $f(v_{||}, v_\perp)$ consists of a Maxwellian core, an isotropic halo in v^{-5}, and a field-aligned beam. See (8) for details. Velocities in units of the thermal core velocity $v_e = (T/m)^{1/2}$.

Since $\Omega_e/(k_{||}v_0) = \Omega_e/\omega \geq 1.5$, the cyclotron-shifted resonant velocities are distant from each other. If we assume $v_0 \sim 20 v_e$ as suggested by Figure 3, then they are separated by at least $30 v_e$, so that only one other resonance ($n = 1$) is important. The others, falling on parts of the distribution where the density of electrons is negligible, can be omitted.

For Langmuir modes with $\omega \lesssim \omega_p$ the separation is close to $30 v_e$. They gain energy from electrons at $v_0 \sim 20 v_e$ and lose energy to electrons at $v_1 = (\omega - \Omega_e)/k_{||} \lesssim -10\ v_e$. From the characteristics of the operator $\hat{L}_n$ and from the resonant condition it can be shown that the diffusion lines are ellipses centered on $v_0/2$: $(v_{||} - v_0/2)^2 + v_\perp^2/2 = C^2$. This feature indicates that the electrons at $v_1 \lesssim -10\ v_e$ are heated mostly in the perpendicular direction. Accordingly, we define the quantity

$$H_\perp(t) = 2 \int_0^t dt' \int \frac{d^3k}{(2\pi)^3} W_k(t')\, \omega_k\, \text{Im } \chi_e(k,\omega_k)|_{n=-1}, \quad (9)$$

which is monitored during the simulation runs to measure the amount of energy that goes into perpendicular heating. The associated cyclotron damping of the oblique Langmuir waves is computed from the Lorentzian tail f_T and (7). Figure 4 shows the damping rate for the ratio $\Omega_e/\omega_p = 1.5$. In $(k_{||}, k_\perp)$ space it forms a clear ridge and damps preferentially modes with angles around 20°. For smaller angles the Bessel function $J_1^2(k_\perp v_\perp/\Omega_e)$ in (7) vanishes; for larger angles the frequency decreases, so that the resonant velocity v_1 shifts to regions of the tail with less particles, resulting in a lesser damping. With greater values of Ω_e/ω_p the ridge of Figure 4 weakens and moves to somewhat larger angles.

For eigenmodes along the resonant line with frequencies $\omega < 0.5\ \omega_p$ the separation between the cyclotron-shifted resonant velocities is larger than $60\ v_e$. Thus only the $n = 0$ term in (7) plays a role. This fact is confirmed by a comparison of Figure 4 with Figure 2, which shows the cyclotron damping to disappear for oblique modes. Note that these modes do transfer energy slowly as a result of (1) their small value of ω_k (see equation (6)) and (2) their large value of k (see equation (7)). However, because $J_0^2(k_\perp v_\perp/\Omega_e)$ windows out the high-$v_\perp$ part of the distribution, the transfer goes from the electrons to the waves as long as a beam-like feature keeps appearing in the field-aligned part of the distribution function.

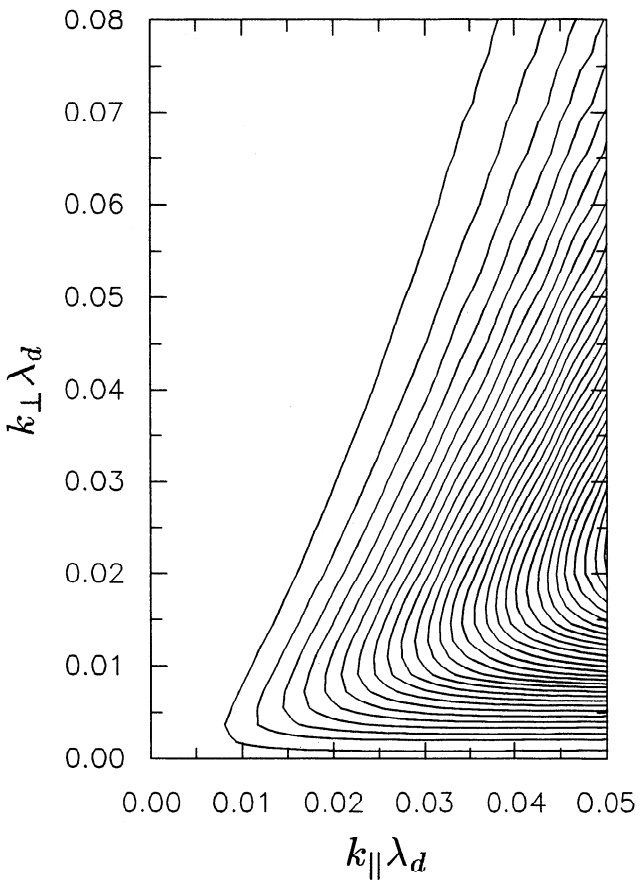

Figure 4. Cyclotron damping in $(k_{||}, k_\perp)$ space. Contours from $5 \times 10^{-6}\omega_p$ up in increments of $5 \times 10^{-6}\omega_p$. Strongest damping $1.45 \times 10^{-4}\omega_p$ at $k_{||}\lambda_d = 0.05$, $k_\perp \lambda_d = 0.02$.

3. Simulation Results

Equations (1) and (2) have been integrated in time with various initial conditions. For $f(v_{||}, v_\perp, t = 0)$ we have used the distribution function depicted in Figure 3, varying the beam and halo characteristics. The spectrum was set to a constant low level. The most interesting cases occur when the beam is partly submerged into the halo. We show results obtained with the following parameter values: $n_T/n_0 = 0.03$, $a/v_e = 4$, $n_b/n_0 = 2.1 \times 10^{-4}$, $U/v_e = 25$, $v_{b||}/v_e = 4$, and $v_{b\perp}/v_e = 3$.

Figure 5 displays the time history of various energy components in nT_e units and a semilog scale. Indicated are the total wave energy (thickest line) $W_{tot} \equiv \int dk_{||} dk_\perp k_\perp (\omega \partial\epsilon/\partial\omega) W_k/(32\pi^3)$, including the mechanical part of the wave motion; and the changes of kinetic energy experienced by the electrons since $t = 0$, which we split into loss in parallel energy (thick line) and gain in perpendicular energy (thin line). The loss in parallel energy $\mathcal{L}_{||}$ is computed directly from the simulation, while the gain $H_\perp(t)$ is calculated with (9). At any given time, energy is conserved, $W_{tot} + H_\perp = \mathcal{L}_{||}$. In addition, the plot indicates the wave electrostatic energy (thin line marked ES), which is proportional to W_{tot} with a factor of proportionality remaining between 2 and 3. One basically distinguishes three phases: (1) a rapid growth in the wave energy associated with a decrease in the parallel kinetic energy, followed by (2) a long period of decay, then (3) growth again associated with an additional loss of parallel kinetic energy. As we shall see, the last phase is dominated by low-frequency, oblique waves in the lower hybrid range. An expanded view of the early history can be seen in Figure 6. The dashed vertical lines indicate specific times, t_1, t_2, and t_3, at which we show below detailed snapshots in $(k_{||}, k_\perp)$ space. Note that around time t_3 the quantity $\mathcal{L}_{||}$ is sligthly decreasing, viz., the electrons are in fact accelerated.

3.1. Phase 1

Figure 7 displays the wave spectrum recorded at time t_1 when the period of linear growth is over and the energy $W_{tot} \sim 10^{-6}$ nT. The five contours denote $W_k/(8\pi n\lambda_d^3 T)$ between 10^{-3} (dotted curve) and 10, one per decade. One observes that the spectrum forms a band that resembles the shape of the resonant line discussed about Figure 2. Waves are growing over a broad range of angles and hence frequencies, including a substantial share of parallel Langmuir waves. The dent in the spectrum around $\theta \sim 20°$ is attributed to the cyclotron damping that reduces the net growth rate of these oblique modes. Compare where the ridge of Figure 4 intercepts the band and note that the spectral intensity is down by 2 orders of magnitude there.

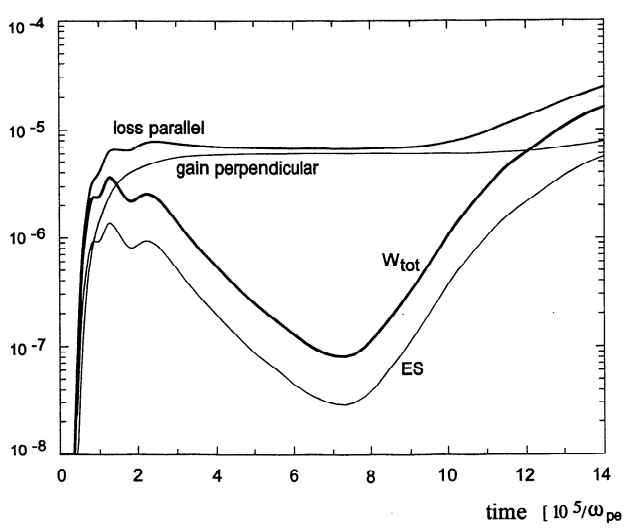

Figure 5. Time history of energy components in units of nT_e: loss in parallel kinetic energy of the electrons since $t = 0$, gain in perpendicular kinetic energy $H_\perp(t)$ (equation (9)), wave total energy W_{tot}, and wave electrostatic energy ES. One distinguishes three phases: rapid wave growth, slow wave decay, and secondary wave growth.

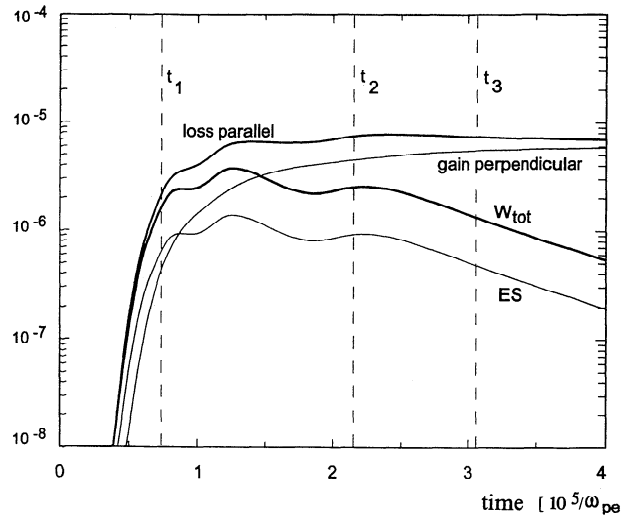

Figure 6. Expanded, early view of Figure 5 in the same format. Times t_1, t_2, and t_3 associated with Figures 7, 8, and 9, respectively, are indicated by dashed vertical lines.

3.2. Phase 2

As the waves react back on the distribution function partially plateauing it, growth shifts to oblique waves. Figure 8 displays the full wavenumber mesh and shows which modes are still growing at time t_2. A dotted line indicates a marginal growth rate of $10^{-7}\omega_p$. Nearly perpendicular, lower hybrid modes grow at a rate of the order of $10^{-6}\omega_p$. Modes with $k_\perp\lambda_d < 0.03$ do not grow any more, in contrast to phase 1, when the Langmuir modes had a typical linear growth rate of several times $10^{-5}\omega_p$. In fact, the oblique Langmuir waves now have a net growth rate that is negative owing to the cyclotron damping; they are damped, and accordingly, $H_\perp(t)$ (Figure 6) shows an increase on the order of $10^{-6}nT$. The spectrum splits thus into purely parallel and very oblique modes. Figure 9 shows an example for time t_3.

During this phase 2 an interesting interplay takes place between oblique and parallel modes. As the former gain in intensity, they quasi-linearly diffuse the electrons, acting more upon the small-gyroradius electrons of the beam than upon the large-gyroradius electrons of the halo. Hence they reduce the positive slopes of f at small $v_\perp$ without correspondingly diminishing the negative slopes of f at large $v_\perp$. As a result the parallel Langmuir waves are no longer "in equilibrium" with the distribution function; for them the reduced distribution function appears to have a negative slope, whereby they slowly decay. This effect shows up in Figure 6, and more dramatically in Figure 5, as a decrease in W_{tot}. We also note from Figure 5 that during the period $3 \times 10^5 < \omega_p t < 6 \times 10^5$ the resonant electrons sligthly gain parallel energy in average. It appears that the acceleration of the halo electrons by the decaying Langmuir modes offsets the deceleration of the field-aligned electrons by the growing oblique modes.

3.3. Phase 3

After $t = 8 \times 10^5\omega_p^{-1}$ the nearly perpendicular and slowly growing modes at $k_\parallel\lambda_d \approx 0.002$ and $k_\perp\lambda_d = 1.5\ k_\perp\rho_e \gtrsim 0.04$ reach an appreciable intensity (here ρ_e denotes the gyroradius of a thermal electron). They begin to dominate W_{tot}, which rises again as seen in Figure 5. While a plateau is dug in the distribution function for the velocity interval $20 \lesssim v_\parallel/v_e \lesssim 25$, steeper gradients form at the fronts of the plateaued region. An example is shown in Figure 10. Growth rates from such a distribution function are the result of a delicate balance of positive and negative slopes. For Langmuir modes this balance leads to intermittent growth and damping (on the order of $10^{-5}\omega_p$). For the nearly perpendicular low-frequency modes the balance leads to a slow but continuous growth (on the order of $10^{-6}\omega_p$). For them the factor $J_0^2(k_\perp v_\perp/\Omega_e)$ windows out the high-$v_\perp$ part of the distribution function. They tap their energy from the low-velocity front about $v_0/v_e \approx 20$ and largely ignore the big gyroradius electrons with $v_\perp/v_e \gtrsim 20$. Eventually, the spectrum is to-

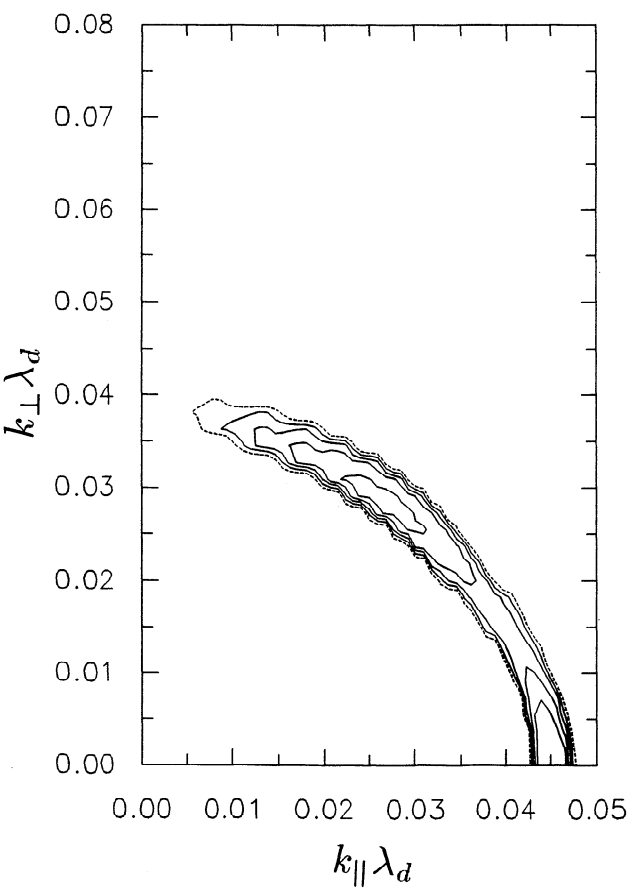

Figure 7. Wave intensity spectrum at the end of the linear growth period ($t_1 = 7.2 \times 10^4\omega_p^{-1}$). Contours of $W_k/(8\pi n\lambda_d^3 T)$ at levels 0.001 (dotted curve), 0.01, 0.1, 1, and 10.

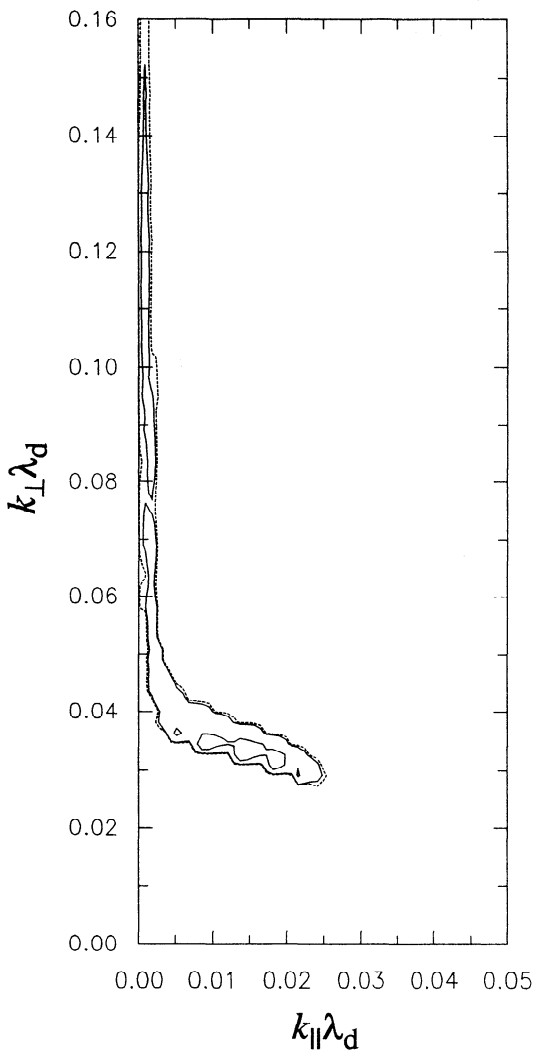

Figure 8. Region of growth in $(k_{||}, k_\perp)$ space at $t_2 = 2.1 \times 10^5 \omega_p^{-1}$. Only oblique modes are now growing. Contours: 10^{-7}(dotted), 10^{-6}, and 10^{-5} in ω_p units.

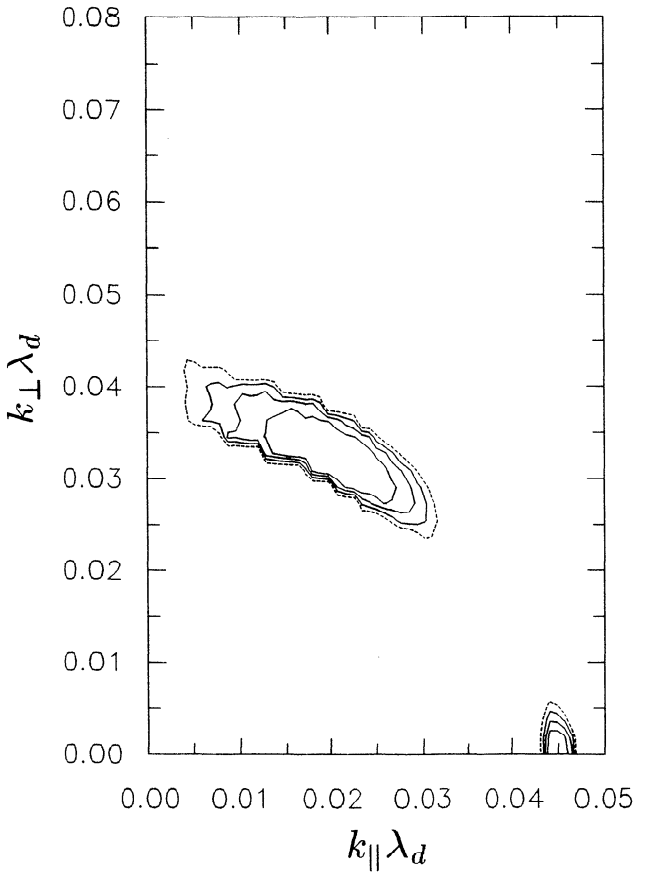

Figure 9. Wave intensity spectrum at $t_3 = 3.04 \times 10^5 \omega_p^{-1}$. The Langmuir component has decreased. Contours of $W_k/(8\pi\, n\lambda_d^3 T)$ at levels: 0.001 (dotted curve), 0.01, 0.1, and 1.

tally dominated by the waves in the lower hybrid range of frequency; the bulk of the spectral power has shifted toward very oblique propagating angles. We stop our simulation run when modes with the largest $k_\perp$ allowed by our mesh reach an appreciable level.

The late spectrum, as visible in Figure 11, consists of roughly two parts: a narrow vertical strip at $k_{||}\lambda_d \approx 0.002$ and a bulk of modes with $k_\perp \lambda_d \lesssim 0.04$. Similar wave levels are found in both parts, $W_k/(8\pi n\lambda_d^3 T) \sim 1$. Analysis shows that the modes of the strip are mainly driven by the front in the distribution function near $v_0 \approx 20\ v_e$ (see Figure 10), whereas the modes with $k_\perp \lambda_d \lesssim 0.04$ are left over from the beam plateauing. The strip has a narrow breadth of $\Delta k_{||} \approx (\Delta v_0/v_0^2)\,\omega_{lh}$ where Δv_0 is the velocity width of the front near $v_0 \approx 20\ v_e$. Since ω_{lh}/ω_p scales as the square root of the mass ratio, it is difficult to design a mesh (even irregular as we have it) that satisfactorily discretizes both Langmuir and lower hybrid waves. On these grounds we have performed another series of runs with the reduced mass ratio $M/m = 100$ and the same distribution function. Results are very similar except for shrunken timescales during phases 2 and 3. Langmuir waves are present for relatively brief times, whereas waves near the lower hybrid frequency end up dominating the spectrum on longer timescales.

4. Discussion

The evolution of the wave intensity and distribution function relies on a balance between the destabilizing effect of the field-aligned beam and the stabilizing effect of the halo. To illustrate how sensitive this balance is, we mention here results obtained by varying the beam density n_b. This parameter controls the part of the distribution function that emerges from the halo. If n_b is reduced from 2.1×10^{-4} to 1.8×10^{-4}, then no Langmuir waves grow at all, and only the modes with large $k_\perp$ are (weakly) unstable. If it is increased to 3.1×10^{-4}, the instability is much stronger; the wave energy peaks at a significantly larger value, $W_{tot} \sim 10^{-4} nT$, and mostly consists of Langmuir modes. Because of the higher

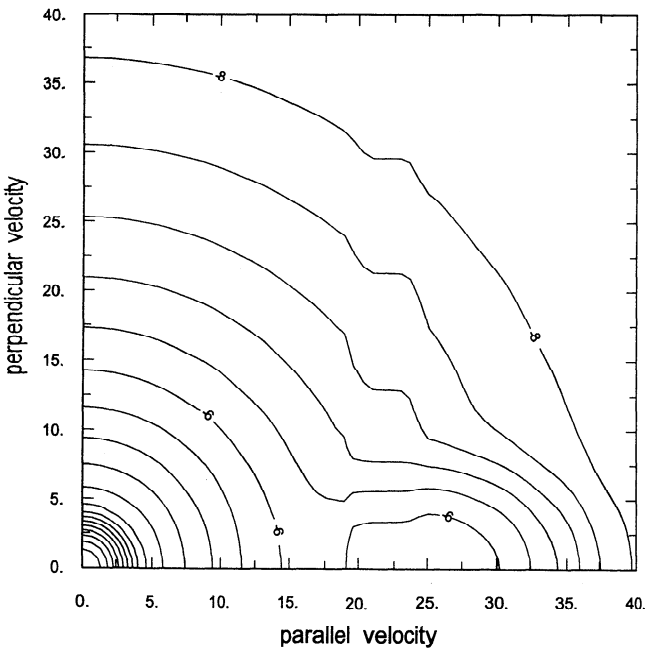

Figure 10. Late distribution function showing the plateaued region. Same contours as in Figure 3. Note the persisting positive slope $\partial f/\partial v_{||} > 0$ at small $v_\perp$.

wave intensity the effect of the cyclotron resonance becomes apparent on contours of the distribution function, which display signatures of perpendicular heating near $v_1 = (\omega - \Omega_e)/k_{||} \lesssim -10\ v_e$. The changes are small, though. Accordingly, the cyclotron damping deviates little from its linear value.

The sensitivity of the results to the balance is significant for the analysis of the observations. The sensitivity may explain the variability of emissions observed: sometimes these are close to the plasma frequency, sometimes they are in the lower hybrid frequency range, and sometimes they are in both ranges simultaneously. Furthermore, the relation between perpendicular width of the beam and width of the halo controls how much the power extends above the lower hybrid frequency.

A late spectrum extracted from the series of runs with $M/m = 100$ is presented in the bottom panel of Figure 12. A format different from Figure 11 is used to facilitate the comparison with measurements taken by sounding rockets; we have reprojected W_k in the $(\omega, k_\perp)$ space, eliminating the independent variable $k_{||}$, which experimentally cannot be directly measured. The frequency ω is normalized to ω_{lh}, and $k_\perp$ is normalized to λ_d^{-1}. Characteristically, the perpendicular wavenumber is shown to increase as the frequency approaches the lower hybrid frequency. The feature is in fact observed in interferometric measurements that attempt to determine the wavelength of the emissions [*Delory*, 1996; *Ergun et al.*, 1991]. In the top panel of Figure 12 we show the experimentally determined dependence of the average perpendicular wavenumber upon the frequency. As the frequency decreases toward the lower hybrid frequency about 3.5 kHz, the wavenumber increases. The

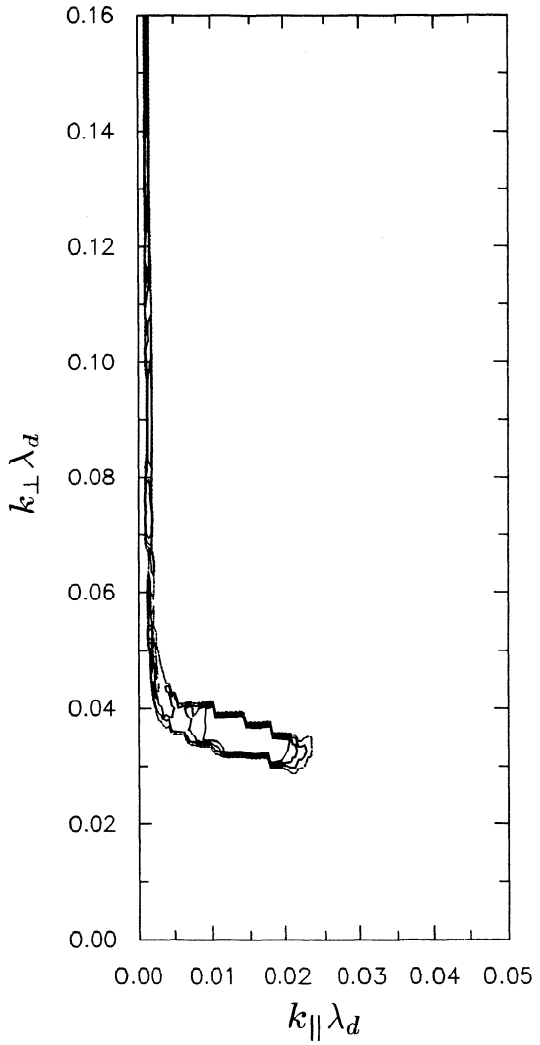

Figure 11. Late wave intensity spectrum. Quasi-perpendicular modes with large $k_\perp$ are excited to levels $W_k/(8\pi n\lambda_d^3 T) \sim 1$, whereas Langmuir modes have disappeared. Same contours as in Figure 9.

dashed curves indicate the resonant lines (like the one displayed in Figure 2) associated with electrons having different parallel kinetic energies $mv_0^2/2$. The spectrum thus appears to be associated with electrons at a specific energy (495 eV in the particular case). In the bottom panel the chain of circles marks the resonant line associated with electrons of the lower velocity front at $v_0/v_e = 19$ (see the distribution function in Figure 10). Similarly, the asterisks mark the upper velocity front at $v_0/v_e = 25$. The feature may thus be a good indication that the observed waves are indeed excited by a field-aligned bump as in our simulations.

A moderate field is typically 20 mV/m rms, which for conditions prevailing at 1000 km altitude ($n = 4000\ \mathrm{cm}^{-3}$, $T = 0.25$ eV) corresponds to an electrostatic energy density $E^2/(8\pi nT) = 10^{-5}$. This value is completely consistent with the wave level in the simulation (see Figure 5). An interesting outcome of the present calculation is that short-wavelength lower hybrid waves with $\lambda \approx 45\lambda_d \approx 3$ m can result from the in-

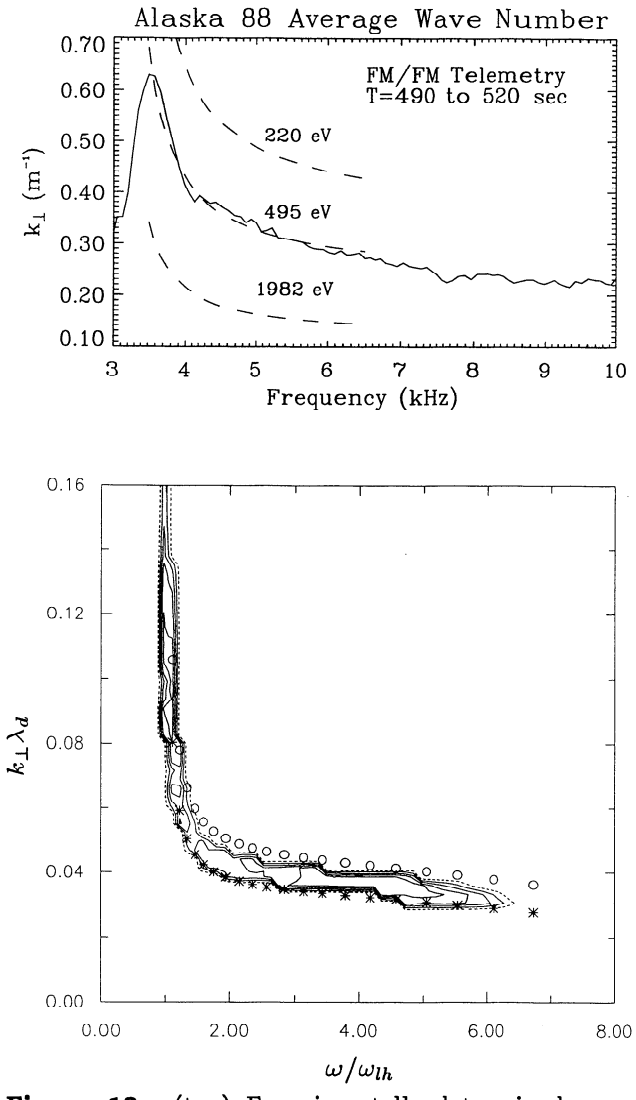

Figure 12. (top) Experimentally determined wavenumber as a function of frequency. (bottom) Late simulation spectrum projected in $(\omega, k_\perp)$ space. Note how the wavenumber increases for frequencies decreasing toward the lower hybrid frequency ω_{lh} (3.5 kHz in the Figure 12 (top)). See text for details.

stability without the recourse to strong turbulence models. The essential ingredient of our quasi-linear model is the halo of energetic electrons that plays a decisive role in shaping the spectrum. At higher altitudes, where the plasma frequency becomes smaller than the gyrofrequency, the effects we discussed in association with the cyclotron damping are expected to disappear. The magnetospheric electrons, though, form an energetic halo, so that we can speculate our main results to hold true.

Extrapolating the simulation results to a realistic mass ratio, we expect the timescale of phases 2 and 3 to be stretched. Between $M/m = 100$ and $M/m = 400$ the timescale increased by approximately a factor of 2. This increase is in line with a transfer rate to the lower hybrid waves proportional to the square root of the mass ratio; from (6) and (7) one obtains roughly $\gamma_{lh} \propto \omega_p \sqrt{m/M}$. Thus stretching the scale of Figure 5 by a factor 2 might give us an idea of what the results would be for a hydrogen plasma, and another factor of 4 would correspond to an oxygen plasma. Future simulations with an improved design of the wavenumber mesh may be able to test the point. The mesh should include an extremely refined grid at small $k_{||}$ and extend further in $k_\perp$, since with time, modes with increasingly large $k_\perp$ are growing. The simulations should also allow for a very large number of time steps, the growth of these modes being increasingly small since they tap energy from fewer and fewer electrons of phase space. Because the quasi-linear model is energy conserving, the wave energy cannot keep growing ad infinitum, such that the curve W_{tot} of Figure 5 will level off eventually. From a pragmatic viewpoint, though, the growth rate may become too small to have a practical significance in the rapidly changing environment of the auroral region. We note in this respect that a time of $10^6\ \omega_p^{-1}$ corresponds to 200 ms for a plasma frequency of 0.6 MHz, while a field-aligned event may typically last from 1 s to a few seconds.

5. Conclusions

We have developed two-dimensional simulations based on the coupled pair of quasi-linear equations. From these and a model of electron distribution function that includes a field-aligned beam embedded in an isotropic halo we draw the following conclusions: (1) The spectrum shifts with time toward increasingly oblique propagation angles. Langmuir waves appear and disappear on timescales of the order of 10 ms. On much longer timescales the lower hybrid waves can indeed grow and drain energy from the beam. (2) Unlike in one dimension there is no asymptotic state in which the waves are "in equilibrium" with a plateaued distribution function: distribution function and spectrum keep evolving. (3) A bump can survive beyond the Langmuir timescale and show up in cuts parallel to the magnetic field.

Acknowledgments. We are indebted to S. Succi, whose thesis work has been expanded into our present code. We thank R. E. Ergun for several discussions. The computations were performed on the Cray C90 of the San Diego Supercomputer Center. The work was supported by NASA grants NAGW-5127 and NAG5-3596, and by NSF grant ATM-9224688.

The Editor thanks J.-P. St-Maurice and R. A. Treumann for their assistance in evaluating this paper.

References

Appert, K., T.M. Tran, and J. Vaclavik, Finite elements approximations for the wave-particle interaction in weakly turbulent plasmas, *Comput. Phys. Commun., 12*, 135, 1976.

Beghin, C., J.L. Rauch, and J.M. Bosqued, Electrostatic plasma waves and HF auroral hiss generated at low altitude, *J. Geophys. Res., 94*, 1359, 1989.

Delory, G.T., Rocket observations of VLF bursts, electron precipitation, and ion heating in the auroral ionosphere, Ph.D thesis, Univ. of Calif., Berkeley, 1996.

Dum, C.T., Anomalous heating by ion sound turbulence, *Phys. Fluids, 21*, 945, 1978.

Dum, C.T., and K. Nishikawa, Two-dimensional simulation studies of the electron beam-plasma instability, *Phys. Plasmas, 1*, 1821, 1994.

Ergun, R.E., E. Klementis, C.W. Carlson, J.P. McFadden, and J.H. Clemmons, Wavelength measurement of the auroral hiss, *J. Geophys. Res., 96*, 21,299, 1991.

Ergun, R.E., G.T. Delory, E. Klementis, C.W. Carlson, J.P. McFadden, I. Roth, and M. Temerin, VLF wave growth from dispersive bursts of field-aligned electron fluxes, *J. Geophys. Res., 98*, 3777, 1993.

Maggs, J.E., Electrostatic noise generated by the auroral electron beam, *J. Geophys. Res., 83*, 3173, 1978.

Maggs, J.E., and W. Lotko, Altitude dependent model of the auroral beam and beam-generated electrostatic noise, *J. Geophys. Res., 86*, 3439, 1981.

McFadden, J.P., C.W. Carlson, M.H. Boehm, and T.J. Hallinan, Field-aligned electron flux oscillations that produce flickering aurora, *J. Geophys. Res, 92*, 11,133, 1987.

Omelchenko, Y.A., V.D. Shapiro, V.I. Shevchenko, M. Ashour-Abdalla, and D. Schriver, Modified lower hybrid fan instability excited by precipitating auroral electrons, *J. Geophys Res., 99*, 5965, 1994.

Parail, V.V., and O.P. Pogutse, Instability of the runaway-electron beam in a tokamak, *Sov. J. Plasma Phys., Engl. Transl., 2*, 126, 1976.

Retterer, J.M., T. Chang, and J.R. Jasperse, Particle acceleration by intense auroral VLF turbulence, in *Physics of Space Plasmas, vol.* 9, edited by T. Chang, G.B. Crew, and J.R. Jasperse, p. 119, Scientific, Cambridge, Mass., 1989.

Roth, I., and M. Temerin, Enrichment of ^{3}He and heavy ions in impulsive solar flares, *Astrophys. J., 477*, 940, 1997.

Serizawa, Y., and C.T. Dum, Nonlocal analysis of finite-beam-driven instabilities. *Phys. Fluids B, 9*, 1821, 1992.

Succi, S., Quasi-linear modeling of lower hybrid current drive and related problems, Ph.D thesis, Polytech. Fed. Sch., Lausanne, Switzerland, 1987.

Temerin, M., and R.L. Lysak, Electromagnetic ion cyclotron-mode (ELF) waves generated by auroral electron precipitation, *J. Geophys. Res., 89*, 2849, 1984.

G. Delory, L. Muschietti, and I. Roth, Space Research Group, Space Sciences Laboratory, University of California, Berkeley, Berkeley, CA 94720-7450. (e-mail: laurent@ssl.berkeley.edu)

(Received June 19, 1997; revised September 4, 1997; accepted September 5, 1997.)